Induced transparency by interference or polarization

Changqing Wang[a], Xuefeng Jiang[a], William R. Sweeney[b,c,d], Chia Wei Hsu[e], Yiming Liu[a], Guangming Zhao[a], Bo Peng[a], Mengzhen Zhang[b,c,d], Liang Jiang[f], A. Douglas Stone[b,c,d], and Lan Yang[a,1]

[a]Department of Electrical and Systems Engineering, Washington University, St. Louis, MO 63130; [b]Department of Applied Physics, Yale University, New Haven, CT 06520; [c]Department of Physics, Yale University, New Haven, CT 06520; [d]Yale Quantum Institute, Yale University, New Haven, CT 06520; [e]Ming Hsieh Department of Electrical Engineering, University of Southern California, Los Angeles, CA 90089; and [f]Pritzker School of Molecular Engineering, University of Chicago, Chicago, IL 60637

Edited by Alexis T. Bell, University of California, Berkeley, CA, and approved December 7, 2020 (received for review June 29, 2020)

Polarization of optical fields is a crucial degree of freedom in the all-optical analogue of electromagnetically induced transparency (EIT). However, the physical origins of EIT and polarization-induced phenomena have not been well distinguished, which can lead to confusion in associated applications such as slow light and optical/quantum storage. Here we study the polarization effects in various optical EIT systems. We find that a polarization mismatch between whispering gallery modes in two indirectly coupled resonators can induce a narrow transparency window in the transmission spectrum resembling the EIT lineshape. However, such polarization-induced transparency (PIT) is distinct from EIT: It originates from strong polarization rotation effects and shows a unidirectional feature. The coexistence of PIT and EIT provides additional routes for the manipulation of light flow in optical resonator systems.

electromagnetically induced transparency | interference | polarization

Coherent processes of light–matter interaction have been utilized to generate electromagnetically induced transparency (EIT) in optical media with Λ-shape energy levels (1, 2). The probability amplitudes of transitions to an excited state are canceled due to the destructive interference between two excitation pathways and thus prevent the absorption of a probe beam. Associated with EIT are the strong normal dispersion and group delay, which play a critical role in applications of slow light and optical storage (3–7). EIT has been widely studied in atomic systems (8–10), superconductors (11, 12), electronics (13), metamaterial/metasurfaces (14, 15), optical resonators (16–22), scattering nanostructures (23), optomechanics (24–27), plasmonics (28–30), etc. Among them, coupled-mode optical platforms, including a single resonator (31–34), directly coupled microresonators (35), and indirectly coupled microresonators (36, 37), have been intensively explored as promising candidates for realizing an all-optical analogue of EIT, due to their advantages of room temperature operation, on-chip integratability, and high tunability for parameter control. The recent study of exceptional-point–assisted transparency (EPAT) (38) offers opportunities for EIT control via chiral eigenstates associated with the exceptional points (EPs) (38–43). While there have been comprehensive explorations into the roles of intermodal coupling, resonance frequencies, optical dissipation rates, and phase factors of propagation, the investigation of another important degree of freedom of light—polarization states of probe fields and optical modes—has been lacking. It is known that the probe- and coupling-field polarizations have a significant influence on the magnitude of EIT in multilevel cascade atomic systems (44–47). In optical systems, the polarization mismatch between the mode fields in different optical devices naturally exists, and it has been demonstrated that the polarization of incident light could modify the transmission lineshape (31). Moreover, transparency and absorption phenomena can also occur in a single resonator supporting overlapping modes with different polarizations (48–50). However, up to now, the distinction between EIT and polarization effects is unclear in two ways: 1) How is EIT affected by the polarization mismatch in different coupled-mode optical systems? And 2) what are the underlying physics of the transparency phenomena caused by polarization effects? To clearly understand the polarization effects and their distinction from EIT is of great significance for properly controlling and using polarization in the induced-transparency phenomena for applications in slow light generation, optical switching, sensing, etc.

Here we report a comprehensive study on the effects of polarization in various configurations for the all-optical analogue of EIT. In particular, we find the polarization-induced transparency (PIT) phenomenon in indirectly coupled resonators, which exhibits a unidirectional feature. This phenomenon is strongly dependent on the polarization mismatch between two cavity modes. Moreover, by exploiting backscattering on the resonator surfaces, the indirectly coupled resonators can function as a hybrid system that involves EIT and PIT simultaneously.

Polarization Effects on EIT in Various Configurations

EIT originates from atomic/molecular systems, such as atomic gases (Fig. 1*A*), which are modeled as Λ-shape energy levels and are composed of a ground state $|1\rangle$, an excited state $|2\rangle$, and a metastable state $|3\rangle$. The decay rate of state $|3\rangle$ is much smaller than that of state $|2\rangle$. The probe (pump) light beam induces the dipole transition $|1\rangle \rightarrow |2\rangle$ ($|2\rangle \rightarrow |3\rangle$), while the dipole transition $|1\rangle \rightarrow |3\rangle$ is forbidden. To generate each

Significance

Electromagnetically induced transparency (EIT) describes the phenomenon that an opaque optical medium becomes transparent due to interference effects. EIT plays a pivotal role in engineering slow light and quantum memory. However, polarization effects could cause similar phenomena and therefore were considered as EIT occasionally. We investigate the polarization effects on EIT in optical resonators and discover a polarization-induced transparency (PIT) phenomenon that the system is transparent in one direction but opaque in the other. PIT results from the polarization effects rather than wave interference and thus fundamentally differs from EIT. This study resolves the confusion between EIT and polarization effects, which is crucial for optical memory design and paves the way to additional techniques for controlling wave propagation.

Author contributions: C.W., X.J., and L.Y. designed research; C.W., X.J., W.R.S., C.W.H., Y.L., G.Z., and L.Y. performed research; C.W., W.R.S., C.W.H., B.P., M.Z., L.J., A.D.S., and L.Y. contributed new reagents/analytic tools; C.W. and Y.L. analyzed data; and C.W., X.J., W.R.S., C.W.H., Y.L., G.Z., B.P., M.Z., L.J., A.D.S., and L.Y. wrote the paper.

The authors declare no competing interest.

This article is a PNAS Direct Submission.

[1]To whom correspondence may be addressed. Email: yang@seas.wustl.edu.

This article contains supporting information online at https://www.pnas.org/lookup/suppl/doi:10.1073/pnas.2012982118/-/DCSupplemental.

Published January 4, 2021.

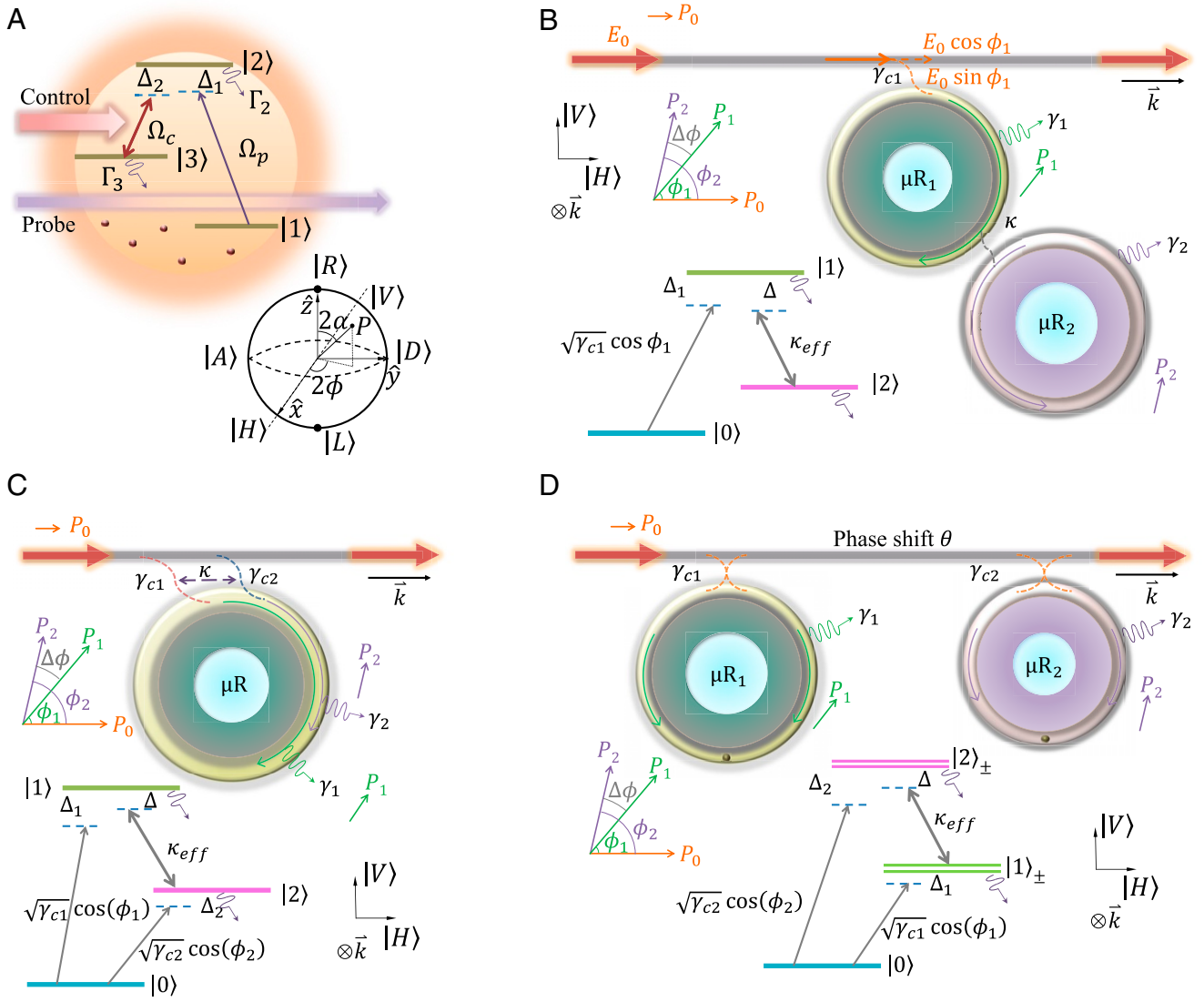

Fig. 1. Polarization effects in different platforms for studying EIT. (*A*) Atomic gas. Ground state, $|1\rangle$; excited state, $|2\rangle$; metastable state, $|3\rangle$. The control and probe light beams have Rabi frequencies Ω_c and Ω_p, respectively. The detuning between $|1\rangle \to |2\rangle$ ($|2\rangle \to |3\rangle$) and the probe (control) light is Δ_1 (Δ_2). For either probe or control light, an arbitrary polarization state P as a superposition of the right and left circular polarization states ($|R\rangle$ and $|L\rangle$) can be represented on a Poincare sphere (51). The right circular, left circular, diagonal linear, and antidiagonal linear polarization states are related to the horizontal and vertical polarization states by $|L,R\rangle = (|H\rangle \pm i\,|V\rangle)/\sqrt{2}$, $|D,A\rangle = (|H\rangle \pm |V\rangle)/\sqrt{2}$. The components of the probe and control light that have a matching polarization will interact with the atomic systems and induce EIT, while the mismatching components will be transparent to the system. (*B*) Directly coupled microresonators. $|0\rangle$, $|1\rangle$, and $|2\rangle$ represent the vacuum state, photons in μR_1, and photons in μR_2, respectively. *Inset* shows the polarization orientations of quasi-TE or quasi-TM modes (52), where $\vec{k}$ is the wavevector. With polarization mismatch, the effective coupling strength between the two resonator modes becomes $\kappa_{eff} = \kappa\cos(\Delta\phi)$. (*C*) A single microresonator with two coupled modes. $|0\rangle$, $|1\rangle$, and $|2\rangle$ representations are similar to *B*. The two modes have disparate quality factors and different polarization states, with the effective coupling strength $\kappa_{eff} = \kappa\cos(\Delta\phi) + \sqrt{\gamma_{c1}\gamma_{c2}}\cos(\phi_1)\cos(\phi_2)$. (*D*) Indirectly coupled microresonators with backscattering. With polarization mismatch, the effective coupling strength between $|1\rangle$ and $|2\rangle$ is given by $\kappa_{eff} = (\gamma_{c1}\gamma_{c2}\kappa_{a21}\kappa_{b12}e^{2i\theta})^{1/4}[\cos(\phi_1)\cos(\phi_2)]^{1/2}$.

dipole transition, certain linearly or circularly polarized light is needed, whose polarization state P is a superposition of the right and left polarization states ($|R\rangle$ and $|L\rangle$); i.e., $P = \cos(\alpha)|R\rangle + e^{-i2\phi}\sin(\alpha)|L\rangle$, where $\alpha \in [0, \pi/2]$ and $\phi \in [0, \pi]$. Thus, P can also be represented by a Bloch sphere (51) as shown in Fig. 1*A*, *Inset*. If the polarization state of the input light does not match the dipole transition, then only the component with aligned polarization orientation will interact with the atomic levels, while the rest will be noninteracting and transparent to the system. As a result, the polarization of the pump light will affect how much control light is effectively coupled to $|2\rangle \to |3\rangle$ and thus determine the effective Rabi frequency (Ω_c). As for the probe light, only the components with the matched polarization will get involved in the EIT process, whereas the other component will be transparent regardless of the coupling between levels $|2\rangle$ and $|3\rangle$ and thus will raise the baseline over the whole transmission spectrum.

In a pair of directly coupled resonators (Fig. 1*B*), the level diagram takes on a very similar form to that of the atomic system mentioned above, if we make the comparison $\Omega_c \leftrightarrow \kappa$, $\Gamma_2 \leftrightarrow \gamma_1 + \gamma_{c1}$, $\Gamma_3 \leftrightarrow \gamma_2 + \gamma_{c2}$, where κ is the coupling strength between the two resonators, and $\gamma_{1,2}$ ($\gamma_{c1,c2}$) are the intrinsic (coupling) loss rates of the resonators μR_1 and μR_2, respectively. The ground state is now replaced by the vacuum state,

while the numbers of photons in μR_1 and μR_2 play the roles of the occupancy of levels $|2\rangle$ and $|3\rangle$, respectively. Whispering gallery modes (WGMs) supported by resonators usually have quasi-transverse-electric (TE) or quasi-transverse-magnetic (TM) polarization states (52). To simplify the analysis, we consider that the input light also has a linear polarization state, and we denote the angle between P_1 (P_2) and P_0 as ϕ_1 (ϕ_2). When the waveguide mode is coupled to μR_1, only the component $E_0 \cos(\phi_1)$ in the orientation of P_1 will be coupled to the cavity mode, while the perpendicular component $E_0 \sin(\phi_1)$ will be transparent and elevate the transmission baseline. On the other hand, when the light couples from μR_1 to μR_2, only the component in the orientation of P_2 will be able to contribute to the mode in μR_2, while the component perpendicular to P_2 will not. The same process happens when the light couples from μR_2 to μR_1. Therefore, the polarization mismatch leads to a reduced coupling efficiency ($\kappa_{eff} = \kappa \cos(\Delta\phi)$). Consequently, the figure of merit of EIT is reduced, and the baseline in the transmission spectrum is raised (detailed analysis in *SI Appendix*, section S1).

In the single-resonator case (Fig. 1*C*), a high-Q mode and low-Q mode overlapping in the frequency spectrum can be coupled to each other directly by mode profile overlap as well as indirectly via a waveguide. The level diagram reveals that both modes are excited by the probe light so that the system is deviated from a perfect EIT model due to the additional absorption into the high-Q mode. Considering different quasi-linear polarization states in the waveguide and the two modes, the effective coupling strength is modified as $\kappa \cos(\Delta\phi) + \sqrt{\gamma_{c1}\gamma_{c2}} \cos(\phi_1) \cos(\phi_2)$, where γ_{c1} (γ_{c2}) denotes the coupling strength between the waveguide and mode 1 (mode 2), κ represents the direct coupling strength between mode 1 and mode 2, ϕ_1 (ϕ_2) is the angle between the polarization of mode 1 (mode 2) and that of the input field, and $\Delta\phi = \phi_2 - \phi_1$. Moreover, it has been reported that the coexisting of resonant modes with orthogonal polarization states can induce transparency even without mode coupling (50).

The optical analogue of EIT can also be realized in indirectly coupled resonators, where the phenomena of EIT and absorption can be controlled by the chiral state of one of the resonators (38). In an indirectly coupled resonator system (Fig. 1*D*), we consider μR_1 and μR_2 to be a high-Q and a low-Q resonator, respectively, both of which support WGMs with backscattering. Each level of the cavity resonance is split into two levels (53, 54) and can be tuned to be degenerate at the EPs (41). The effective coupling between the modes in two cavities is given by $(\gamma_{c1}\gamma_{c2}\kappa_{a21}\kappa_{b12} e^{2i\theta})^{1/4} [\cos(\phi_1)\cos(\phi_2)]^{1/2}$, which vanishes at one type of EP ($\kappa_{a21} = 0$) and exists at the other ($\kappa_{a21} \neq 0$). The transition $|0\rangle \rightarrow |1\rangle$ can be neglected when it is much smaller than the transition $|0\rangle \rightarrow |2\rangle \rightarrow |1\rangle$. However, if P_1 is different from P_0 and $\gamma_{c1} \gtrsim \gamma_1$, the polarization of light passing μR_1 can be greatly rotated, which significantly affects the transition $|0\rangle \rightarrow |2\rangle$ and gives rise to a reduced absorption at μR_2. Such a polarization effect will not only reduce the efficiency of the EIT configuration, but also lead to another kind of induced transparency phenomenon, which we will discuss in detail.

In all of the above cases, the polarization mismatch in the control light or mode coupling reduces the efficiency of EIT, but does not break the fundamental conditions of EIT. Similarly, the EIT efficiency is reduced by the polarization mismatch of the probe light in the first two cases. Nevertheless, in the last two cases, the polarization mismatch between the input light and the mode will induce fundamentally different phenomena.

PIT

The most intriguing polarization-induced phenomenon can be seen from the indirect coupling scheme. Consider two indirectly coupled resonators (μR_1 and μR_2) supporting clockwise (CW) and counterclockwise (CCW) WGMs with quality factors of Q_1 and Q_2 ($Q_1 \gg Q_2$). We follow the notation used in Fig. 1*D*. The quasi-linear polarization states P_1 and P_2 of the CW modes (52) in μR_1 and μR_2 form angles of ϕ_1 and ϕ_2 relative to the polarization orientation of the input light (P_0). In describing the full scattering properties of the system, we introduce the relationship between the input and output fields as

$$\begin{pmatrix} \lambda_x' \\ \lambda_y' \\ \rho_x' \\ \rho_y' \end{pmatrix} = S \begin{pmatrix} \lambda_x \\ \lambda_y \\ \rho_x \\ \rho_y \end{pmatrix}, \quad [1]$$

with $\lambda_{x(y)}$ and $\rho_{x(y)}$ being the $x(y)$ polarization components of the left- and right-incident field amplitudes, respectively. The $\lambda'_{x(y)}$ and $\rho'_{x(y)}$ are the $x(y)$ polarization components of the outcoming field amplitudes from the left and right ports, respectively. We now consider $t_{1,2}$ to be the transmission matrices of each individual resonator. The reflections to the left (right) are represented by r_{1L} (r_{1R}) and r_{2L} (r_{2R}) for μR_1 and μR_2, respectively. The scattering matrix can be written as

$$S = \begin{pmatrix} r_L & t_L \\ t_R & r_R \end{pmatrix}, \quad [2]$$

with

$$r_L = U_1^T t_1^T U_2^T \left(1 - r_{2L} U_2 r_{1R} U_2^T\right)^{-1} r_{2L} U_2 t_1 U_1 + U_1^T r_{1L} U_1, \quad [3]$$

$$r_R = t_2 U_2 r_{1R} U_2^T \left(1 - r_{2L} U_2 r_{1R} U_2^T\right)^{-1} t_2^T + r_{2R}, \quad [4]$$

$$t_R^T = t_L = U_1^T t_1^T U_2^T \left(1 - r_{2L} U_2 r_{1R} U_2^T\right)^{-1} t_2^T, \quad [5]$$

where $U_{1,2}$ are unitary matrices encoding the polarization mixing during the light propagation from the input port to μR_1 and the propagation between μR_1 and μR_2 (due to, for example, polarization controllers inserted onto the waveguide) (*SI Appendix*, section S2).

To see the phenomena purely induced by polarization effects, we investigate a simple case that the resonators have no backscattering in their mode volumes and support degenerate WGMs. As a result, the system is composed of cascaded resonators, where the second resonator is influenced by the light coming out of the first resonator, while the first resonator is not influenced by the second one (55, 56). The system is described by the S matrix

$$S = \begin{pmatrix} 0 & (t_2 U_2 t_1 U_1)^T \\ t_2 U_2 t_1 U_1 & 0 \end{pmatrix}. \quad [6]$$

$t_{1,2}$ can be calculated using the temporal coupled-mode theory (TCMT)

$$t_{1,2} = 1 - 2i W_{1,2}^{\dagger} (\omega - H_{\text{eff}\,1,2})^{-1} W_{1,2}, \quad [7]$$

where the effective Hamiltonian is

$$H_{\text{eff}\,1,2} = \omega_{1,2} - i\gamma_{1,2}/2 - i W_{1,2} W_{1,2}^{\dagger}, \quad [8]$$

and the coupling matrix is

$$W_{1,2} = \sqrt{\frac{\gamma_{c1,2}}{2}}\left(e^{i\delta_{1,2}}\cos\phi_{1,2}\, e^{i\chi_{1,2}}\sin\phi_{1,2}\right), \qquad [9]$$

with $\delta_{1,2}$ and $\chi_{1,2}$ being the phases related to the coupling coefficients. The forward and backward transmission spectra can be obtained by solving Eqs. **6**–**9** (*SI Appendix*, section S3).

To show polarization-induced phenomena, we design an experimental setup where a high-Q microtoroid resonator (μR_1) and a low-Q microtoroid resonator (μR_2) are coupled to a taper fiber waveguide. We investigate the case that P_0 aligns with P_2, which are both in the x direction. The angle between P_1 and P_2 is set to be ϕ achieved by a polarization controller (PC) applied onto the waveguide between them. When only μR_2 is coupled to the taper, a single Lorentzian dip appears in the transmission spectrum. However, when μR_1 is also coupled to the taper (Fig. 2*A*), a narrow transparency window appears in the forward transmission spectrum (Fig. 2*B*). This phenomenon originates from the polarization discrepancy when the field travels from the waveguide (E) to μR_1 or vice versa. When E encounters μR_1, only the component with the polarization orientation in the direction of P_1 interacts with the resonator and passes with ratio t_1 (t_1 is dependent on the coupling condition and laser frequency detuning), while the perpendicular component gets fully transmitted. Thus the light passing μR_1 will have a polarization state significantly changed from P_0, which cannot be completely absorbed by μR_2. Under the special condition that both resonators are critically coupled to the waveguide and the laser frequency detuning is zero, the polarization effect can be simply explained by the polarization decomposition shown by the vectors in Fig. 2*A*. The modified absorption spectrum of the system is accompanied by a change of dispersion, based on the connection of real and imaginary parts of the response function governed by the Kramers–Kronig relations. The group delay of both x and y polarization components of the forwardly propagating field can be calculated by (27)

$$\tau_{x,y} = -\frac{d\left[arg\left(t_{x,y}\right)\right]}{d\omega}, \qquad [10]$$

where ω is the frequency of the input optical field, and the transmission rates are related to the S matrix in Eq. **6** by $t_x = S_{3,1}$ and $t_y = S_{4,1}$. The numerical results show that the x polarization component of the output exhibits a large group delay within a narrow spectrum window, while the y polarization component of the output shows group advance (Fig. 2*C*). Therefore, slow and fast light features are associated with different polarization states of the output light. The principle of the induced transparency phenomenon is different from EIT and EPAT, and thus we name it PIT.

Furthermore, the PIT is unidirectional. In particular, when μR_2 is critically coupled to the taper, i.e., $\gamma_{c2} = \gamma_2$, the backward transmission spectrum displays a pure absorption dip (Fig. 2 *D* and *E*), because the field at zero detuning is fully absorbed by μR_2 before probing μR_1. In addition, the modulation on the group velocity is also found to be unidirectional, as the y polarization component of the backward-propagating light (when the polarization of the input is still in the x direction) exhibits group delay instead of group advance (Fig. 2*F*). The unidirectionality in the transmission spectrum and dispersion uniquely associated with PIT can serve as a criterion for distinguishing between EIT and PIT in this scheme. It is worth noting that the unidirectionality of PIT does not violate reciprocity; the S matrix here has

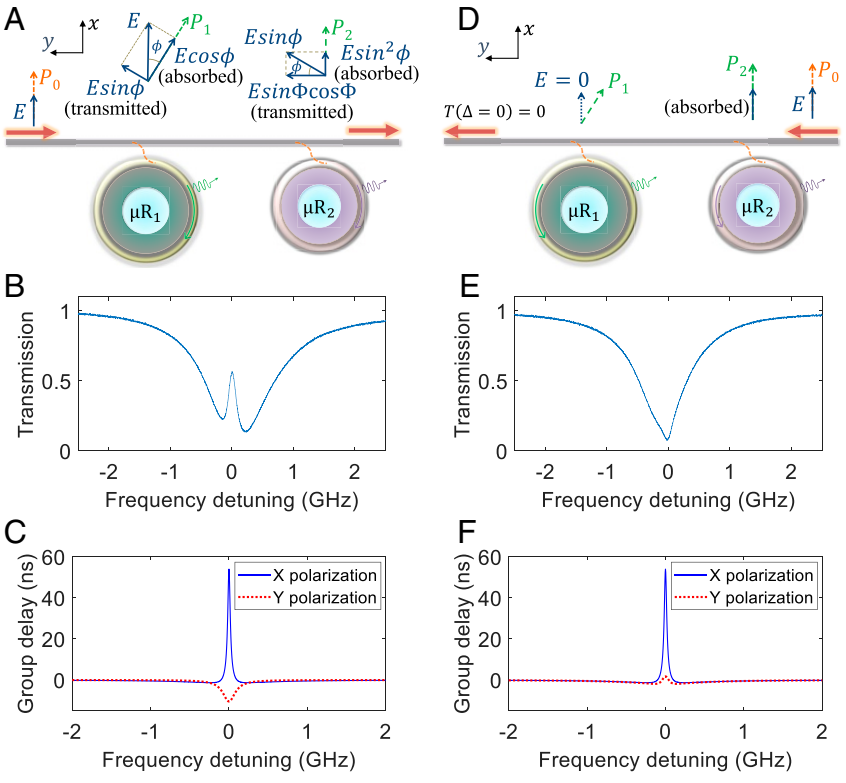

Fig. 2. Unidirectional PIT. (*A* and *D*) Schematic diagrams of a single-mode waveguide coupled to two microresonators with no backscattering (μR_1 and μR_2). The vectors representing the polarization states explain the polarization decomposition during light propagation in the case that both resonators are critically coupled to the waveguide and the laser frequency is identical to the resonant frequencies of the resonators. (*B* and *E*) Experimental results of (*B*) forward and (*E*) backward transmission spectra. (*C* and *F*) Calculated group delay for (*C*) forward and (*F*) backward propagation. $\phi = 0.25\pi$ for results in *B*, *C*, *E*, and *F*.

reciprocity symmetry. This symmetry does not imply that, for a given input polarization, the total left to right output equals the total right to left output summed over polarizations (*SI Appendix*, section S3).

We then study how the polarization state of μR_1 affects the forward transmission spectrum. The polarization of the input laser is controlled by a polarization controller (PC1). We apply another polarization controller (PC2) to the intermediate fiber between the two resonators, so that the polarization state of the light propagating through this region can be controlled manually. After initially aligning P_0 to P_2 by PC2, we can apply a linear rotation of PC1 and PC2 in opposite directions to equivalently adjust the P_1, while ensuring that P_0 and P_2 remain aligned (see *Materials and Methods* for details). P_1 is recorded by separately characterizing the transmission spectrum of μR_1. Starting from the condition $P_1 = P_2 = P_0$, we observe pure absorption in the transmission spectrum as a result of the sum of light absorption by both resonators. With the effective change of the orientation of P_1 (rotation angle $\Delta\phi$), the absorption rate of μR_1 is gradually reduced, accompanied by the appearance of narrow peaks in the spectrum (Fig. 3*A*). The peak at zero detuning undergoes oscillation with an increase of $\Delta\phi$, reaching the maximum around $\Delta\phi = 0.25\pi$ (Fig. 3*B*).

The effect of polarization can also be modulated by the waveguide–resonator coupling strengths γ_{c1} and γ_{c2}. This is shown by studying the variation of transmission at the zero detuning versus the change of P_1 under different γ_{c1} and γ_{c2}. When the coupling strength between the high-Q resonator μR_1 and the taper is increased and pushed into the overcoupling regime, one can find a higher-transparency peak (green dashed curve in Fig. 3*C*) compared to the critical coupling situation (black solid curve in Fig. 3*C*). This owes to the fact that the transmission coefficient $t_1(\Delta) = \frac{i\Delta-(\gamma_1-\gamma_{c1})/2}{i\Delta-(\gamma_1+\gamma_{c1})/2}$ at zero detuning ($\Delta = 0$) becomes negative in the strong coupling regime ($\gamma_{c1} > \gamma_1$), introducing a π phase shift to the P_1 component of the transmitted field in the waveguide, which significantly rotates the polarization of the total field passing μR_1. On the other hand, PIT is also influenced by the coupling strength between μR_2 and the waveguide. Among all coupling conditions, the highest peak appears around $\Delta\phi = \pi/4$, and a local minimum shows up at $\Delta\phi = \pi/2$; namely P_1 is perpendicular to P_2 and μR_1 is decoupled from the optical path (Fig. 3*C*). Yet the contrasts of the transparency window, which mark the efficiency of PIT, are smaller in the cases of undercoupling and overcoupling than in the critical coupling case. Thus based on the discussion above, PIT is optimized when μR_1 is overcoupled to the taper and μR_2 is critically coupled to the taper.

Hybrid System for EIT and PIT

We finally investigate indirectly coupled resonators with backscattering, where EIT and PIT could appear simultaneously. By steering μR_1 to EPs, transparency or absorption occurs depending on the type of EPs classified by the chirality of eigenstates (38). For EP_- where the eigenmode is in the CCW direction and has chirality -1, the interference is "switched off" resulting in exceptional-point–assisted absorption (EPAA). For EP_+ at which the eigenmode is in the CW direction with chirality $+1$, the destructive interference leads to EPAT. Here we find that the polarization mismatch $\Delta\phi$ could significantly modify the transmission spectra (*SI Appendix*, section S4). With the initial splitting of μR_1, under weak coupling between μR_1 and the taper, the transmission shows a splitting absorption window when $\Delta\phi = 0$, but exhibits a splitting transparency window when $\Delta\phi = \pi/4$ (Fig. 4*A*). When μR_1 is steered to EP_- (or EP_+), the lineshape of EPAA (or EPAT) appears when $\Delta\phi = 0$ (Fig. 4 *B* and *C*). But with the polarization mismatch, a large transparency window can be induced in the forward transmission spectrum in both the cases of EPAA and EPAT.

In experiments, we choose a microtoroid (μR_1) and a microdisk (μR_2) resonator with strong backscattering and polarization mismatch. With initial mode splitting in both resonators,

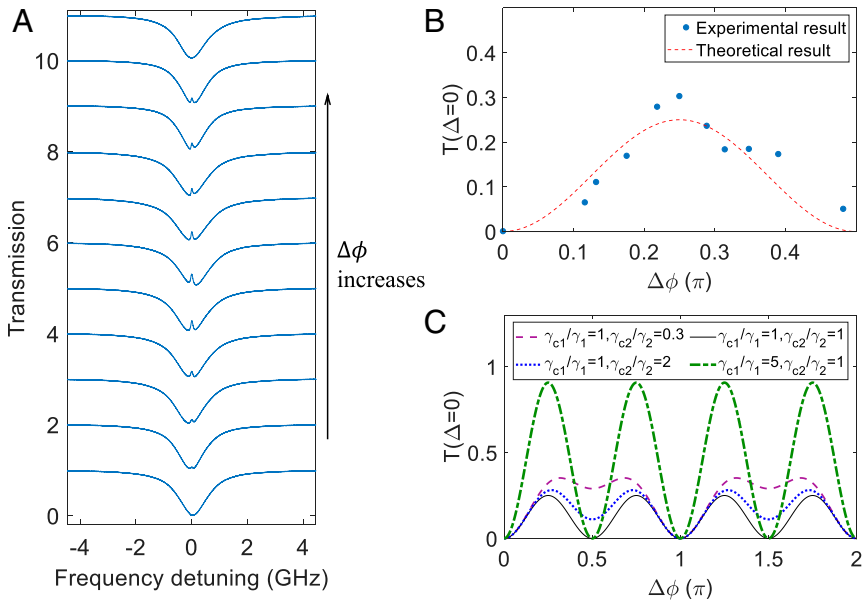

Fig. 3. Effects of the polarization mismatch between two resonators and the resonator–taper coupling strengths on PIT. (*A*) Experimentally measured transmission spectra of two indirectly coupled microtoroid resonators (μR_1, high Q; μR_2, low Q). The polarization state of μR_2 is aligned with that of the incident light. The polarization of μR_1 is kept at linear polarization and rotates by $\Delta\phi$ with respect to the polarization state of μR_2. From bottom to top, $\Delta\phi$ increases from 0 to $\pi/2$. (*B*) Transmission at zero detuning versus the angle change of the polarization orientation of μR_1. The blue circles are the experimental results from *A*. The red dotted line is the theoretical result with $\gamma_{c1} = \gamma_1$ and $\gamma_{c2} = \gamma_2$. (*C*) Theoretical results of the transmission at zero detuning versus the change of polarization state of μR_1 at different resonator–waveguide coupling strengths.

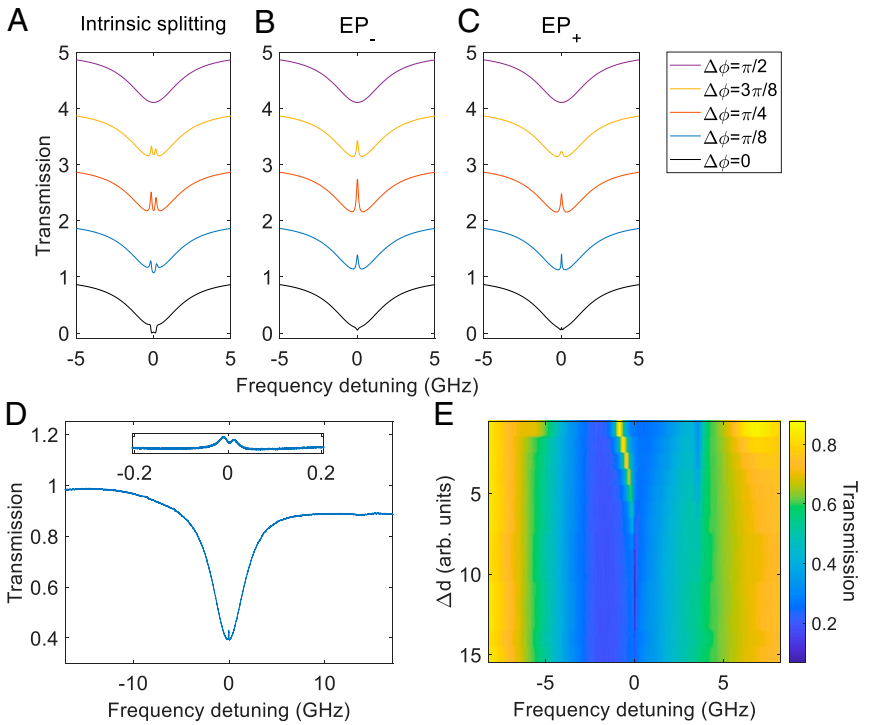

Fig. 4. Polarization effect in indirectly coupled resonators with backscattering. (*A*–*C*) Theoretical results for the mode-splitting case (*A*), the EP$_-$ case (*B*), and the EP$_+$ case (*C*), with different relative polarization angles ($\Delta\phi$). The transmission values are shifted by 1 in each curve for visual comparison. (*D*) Experimental transmission spectrum when there is a mode splitting in μR$_1$. *Inset* shows a close-up of the transmission spectrum around the zero detuning. (*E*) Experimental transmission spectra with the change of the gap between μR$_1$ and the taper (Δd).

a transparency window with splitting is observed (Fig. 4*D*). The peak becomes larger with increased coupling strength between μR$_1$ and the fiber taper (Fig. 4*E*).

Discussion

The physical phenomena and processes discussed above shed light on the distinction between EIT and PIT. First, the all-optical analogue of EIT in linear optical systems is the direct result of interference in the optical paths and has the Λ-type level structure, whereas the occurrence of PIT is irrelevant to interference effects. Second, while EIT depends on large intermodal coupling, PIT occurs in the absence of it and can display a large transparency window based on the strong polarization rotation effect enabled by the microresonators. Third, PIT is accompanied by a unidirectional behavior, while EIT occurs for transmission in both directions.

Such a clarification is important not only in terms of accuracy of physical concepts, but also from the perspective of applications. Slow light application relies on group delay in optical signal, which can be realized by the all-optical analogue of EIT, EPAT, optomechanically induced transparency (OMIT) (24–27), and Brillouin-scattering–induced transparency (BSIT) (21, 22), etc. With a different mechanism from EIT, PIT offers an alternative approach to manipulate the group index of optical media for the control of slow light which is direction and polarization dependent. Furthermore, the unidirectionality associated with PIT enables directional control of light transport without the need of any nonlinear elements or external control, which can potentially benefit optical information processing in on-chip all-optical devices, systems, and networks.

Materials and Methods

Control of the Polarization of One Resonator by a Polarization Controller. In the experiments for Fig. 3 in the main text, we intend to rotate the polarization of the mode in μR$_1$ without physically changing the optical structure. After initially aligning P_0 to P_2 by PC2, we apply a linear rotation of PC1 and PC2 in opposite directions. We now prove that this method can equivalently adjust P_1 without breaking the alignment between P_0 and P_2. The rotation of P_1 and P_2 in opposite directions but by the same degree ensures that any rotation of PC2 described by a rotation matrix U is accompanied with a rotation $U^\dagger$ on PC1, so that the output vector from the right port becomes

$$\begin{pmatrix}\rho_x'\\ \rho_y'\end{pmatrix} = t_2 U t_1 U^\dagger \begin{pmatrix}\lambda_x\\ \lambda_y\end{pmatrix}. \quad [11]$$

This operation can be regarded as applying a rotation to t_1; that is,

$$U t_1 U^\dagger = 1 - 2i(UW_1^\dagger)(\omega - H_{\text{eff}\,1})^{-1}(W_1 U^\dagger), \quad [12]$$

which is equivalent to the rotation of the coupling matrix W, or the polarization state of μR$_1$, by U. Thus, an arbitrary polarization mismatch between the two resonators can be chosen.

In the experiments, the drift of polarization is overcome by carefully fixing the position of the intermediate fiber between resonators. Polarization-maintained fibers can be utilized to further improve the polarization stability.

Data Availability. All data are included in the article and *SI Appendix*.

ACKNOWLEDGMENTS. This work was supported by NSF Grant EFMA-1641109 and Army Research Office (ARO) Grants W911NF1710189 and W911NF1910234. A.D.S. acknowledges the support of NSF Grant DMR-1743235. L.J. acknowledges the support of the Packard Foundation (2013-39273). C.W. acknowledges the fellowship support through the McDonnell International Scholars Academy.

1. M. Fleischhauer, A. Imamoglu, J. P. Marangos, Electromagnetically induced transparency: Optics in coherent media. *Rev. Mod. Phys.* **77**, 633 (2005).
2. J. P. Marangos, Electromagnetically induced transparency. *J. Mod. Optic.* **45**, 471–503 (1998).
3. M. Lukin, A. Imamoğlu, Controlling photons using electromagnetically induced transparency. *Nature* **413**, 273–276 (2001).
4. B. Wu *et al.*, Slow light on a chip via atomic quantum state control. *Nat. Photon.* **4**, 776–779 (2010).

5. L. V. Hau, S. E. Harris, Z. Dutton, C. H. Behroozi, Light speed reduction to 17 meters per second in an ultracold atomic gas. *Nature* **397**, 594–598 (1999).
6. X. Zhou *et al.*, Slowing, advancing and switching of microwave signals using circuit nanoelectromechanics. *Nat. Phys.* **9**, 179–184 (2013).
7. K. M. Beck, M. Hosseini, Y. Duan, V. Vuletić, Large conditional single-photon cross-phase modulation. *Proc. Natl. Acad. Sci. U.S.A.* **113**, 9740–9744 (2016).
8. R. Röhlsberger, H. C. Wille, K. Schlage, B. Sahoo, Electromagnetically induced transparency with resonant nuclei in a cavity. *Nature* **482**, 199–203 (2012).
9. S. E. Harris, J. E. Field, A. Imamoğlu, Nonlinear optical processes using electromagnetically induced transparency. *Phys. Rev. Lett.* **64**, 1107–1110 (1990).
10. K. J. Boller, A. Imamoğlu, S. E. Harris, Observation of electromagnetically induced transparency. *Phys. Rev. Lett.* **66**, 2593–2596 (1991).
11. P. M. Anisimov, J. P. Dowling, B. C. Sanders, Objectively discerning Autler-Townes splitting from electromagnetically induced transparency. *Phys. Rev. Lett.* **107**, 163604 (2011).
12. A. A. Abdumalikov Jr *et al.*, Electromagnetically induced transparency on a single artificial atom. *Phys. Rev. Lett.* **104**, 193601 (2010).
13. C. Garrido Alzar, M. Martinez, P. Nussenzveig, Classical analog of electromagnetically induced transparency. *Am. J. Phys.* **70**, 37–41 (2002).
14. N. Papasimakis, V. A. Fedotov, N. I. Zheludev, S. L. Prosvirnin, Metamaterial analog of electromagnetically induced transparency. *Phys. Rev. Lett.* **101**, 253903 (2008).
15. P. Tassin *et al.*, Electromagnetically induced transparency and absorption in metamaterials: The radiating two-oscillator model and its experimental confirmation. *Phys. Rev. Lett.* **109**, 187401 (2012).
16. Q. Xu, P. Dong, M. Lipson, Breaking the delay-bandwidth limit in a photonic structure. *Nat. Phys.* **3**, 406–410 (2007).
17. M. F. Yanik, W. Suh, Z. Wang, S. Fan, Stopping light in a waveguide with an all-optical analog of electromagnetically induced transparency. *Phys. Rev. Lett.* **93**, 233903 (2004).
18. M. F. Limonov, M. V. Rybin, A. N. Poddubny, Y. S. Kivshar, Fano resonances in photonics. *Nat. Photon.* **11**, 543–554 (2017).
19. K. Totsuka, N. Kobayashi, M. Tomita, Slow light in coupled-resonator-induced transparency. *Phys. Rev. Lett.* **98**, 213904 (2007).
20. Y. C. Liu, B. B. Li, Y. F. Xiao, Electromagnetically induced transparency in optical microcavities. *Nanophotonics* **6**, 789–811 (2017).
21. C. H. Dong *et al.*, Brillouin-scattering-induced transparency and non-reciprocal light storage. *Nat. Commun.* **6**, 6193 (2015).
22. J. Kim, M. C. Kuzyk, K. Han, H. Wang, G. Bahl, Non-reciprocal Brillouin scattering induced transparency. *Nat. Phys.* **11**, 275–280 (2015).
23. C. W. Hsu, B. G. DeLacy, S. G. Johnson, J. D. Joannopoulos, M. Soljacic, Theoretical criteria for scattering dark states in nanostructured particles. *Nano Lett.* **14**, 2783–2788 (2014).
24. A. H. Safavi-Naeini *et al.*, Electromagnetically induced transparency and slow light with optomechanics. *Nature* **472**, 69–73 (2011).
25. S. Weis *et al.*, Optomechanically induced transparency. *Science* **330**, 1520–1523 (2010).
26. C. Dong, V. Fiore, M. C. Kuzyk, H. Wang, Optomechanical dark mode. *Science* **338**, 1609–1613 (2012).
27. H. Lü., C. Wang, L. Yang, H. Jing, Optomechanically induced transparency at exceptional points. *Phys. Rev. Appl.* **10**, 014006 (2018).
28. N. Liu *et al.*, Plasmonic analogue of electromagnetically induced transparency at the drude damping limit. *Nat. Mater.* **8**, 758–762 (2009).
29. G. C. Dyer *et al.*, Induced transparency by coupling of Tamm and defect states in tunable terahertz plasmonic crystals. *Nat. Photon.* **7**, 925–930 (2013).
30. R. Taubert, M. Hentschel, J. Kastel, H. Giessen, Classical analog of electromagnetically induced absorption in plasmonics. *Nano Lett.* **12**, 1367–1371 (2012).
31. B. B. Li *et al.*, Experimental observation of Fano resonance in a single whispering-gallery microresonator. *Appl. Phys. Lett.* **98**, 021116 (2011).
32. G. Zhao *et al.*, Raman lasing and Fano lineshapes in a packaged fiber-coupled whispering-gallery-mode microresonator. *Sci. Bull.* **62**, 875–878 (2017).
33. Y. Zheng *et al.*, Optically induced transparency in a micro-cavity. *Light Sci. Appl.* **5**, e16072 (2016).
34. Y. F. Xiao, L. He, J. Zhu, L. Yang, Electromagnetically induced transparency-like effect in a single polydimethylsiloxane-coated silica microtoroid. *Appl. Phys. Lett.* **94**, 231115 (2009).
35. B. Peng, Ş. K. Özdemir, W. Chen, L. F NoriYang, What is and what is not electromagnetically induced transparency in whispering-gallery microcavities. *Nat. Commun.* **5**, 5082 (2014).
36. B. B. Li *et al.*, Experimental controlling of Fano resonance in indirectly coupled whispering-gallery microresonators. *Appl. Phys. Lett.* **100**, 021108 (2012).
37. Q. Xu *et al.*, Experimental realization of an on-chip all-optical analogue to electromagnetically induced transparency. *Phys. Rev. Lett.* **96**, 123901 (2006).
38. C. Wang *et al.,* Electromagnetically induced transparency at a chiral exceptional point. *Nat. Phys.* **16**, 334–340 (2020).
39. M. A. Miri, A. Alù, Exceptional points in optics and photonics. *Science* **363**, eaar7709 (2019).
40. J. Wiersig, Chiral and nonorthogonal eigenstate pairs in open quantum systems with weak backscattering between counterpropagating traveling waves. *Phys. Rev.* **89**, 012119 (2014).
41. B. Peng *et al.*, Chiral modes and directional lasing at exceptional points. *Proc. Natl. Acad. Sci. U.S.A.* **113**, 6845–6850 (2016).
42. P. Miao *et al.*, Orbital angular momentum microlaser. *Science* **353**, 464–467 (2016).
43. C. W. Hsu. W. R. Sweeney, S. Rotter, A. D. Stone, Perfectly absorbing exceptional points and chiral absorbers. *Phys. Rev. Lett.* **122**, 093901 (2019).
44. S. Wielandy, A. L. Gaeta, Coherent control of the polarization of an optical field. *Phys. Rev. Lett.* **81**, 3359–3362 (1998).
45. R. Drampyan, S. Pustelny, W. Gawlik, Electromagnetically induced transparency versus nonlinear Faraday effect: Coherent control of light-beam polarization. *Phys. Rev.* **80**, 033815 (2009).
46. B. Wang *et al.*, Controlling the polarization rotation of an optical field via asymmetry in electromagnetically induced transparency. *Phys. Rev.* **73**, 051801 (2006).
47. D. McGloin, M. H. Dunn, D. J. Fulton, Polarization effects in electromagnetically induced transparency. *Phys. Rev.* **62**, 053802 (2000).
48. A. Rosenberger, "EIT analogs using orthogonally polarized modes of a single whispering-gallery microresonator" in *Advances in Slow and Fast Light VI*, S. M. Shahriar, F. A. Narducci, Eds. (International Society for Optics and Photonics, 2013), vol. 8636, p. 863602 .
49. A. Rosenberger, "Comparison of methods for achieving induced transparency or absorption with pulse delay or advancement in a single microresonator" in *Slow Light, Fast Light, and Opto-Atomic Precision Metrology IX*, S. M. Shahriar, J. Scheuer, Eds. (International Society for Optics and Photonics, 2016), vol. 9763, p. 97631E.
50. K. V. Bui, A. Rosenberger, "Experimental study of induced transparency or absorption and slow or fast light using orthogonally polarized whispering gallery modes of a single microresonator" in *Slow Light, Fast Light, and Opto-Atomic Precision Metrology IX*, S. M. Shahriar, J. Scheuer, Eds. (International Society for Optics and Photonics, 2016), vol. 9763, p. 97630W.
51. J. A. Jones, A. J. D'Addario, B. L. Rojec, G. Milione, E. J. Galvez, The Poincaré-sphere approach to polarization: Formalism and new labs with Poincaré beams. *Am. J. Phys.* **84**, 822–835 (2016).
52. B. Min, L. Yang, K. Vahala, Perturbative analytic theory of an ultrahigh-Q toroidal microcavity. *Phys. Rev.* **76**, 013823 (2007).
53. J. Zhu *et al.*, On-chip single nanoparticle detection and sizing by mode splitting in an ultrahigh-Q microresonator. *Nat. Photon.* **4**, 46–49 (2010).
54. Ş. K. Özdemir *et al.*, Highly sensitive detection of nanoparticles with a self-referenced and self-heterodyned whispering-gallery Raman microlaser. *Proc. Natl. Acad. Sci. U.S.A.* **111**, E3836–E3844 (2014).
55. C. Gardiner, Driving a quantum system with the output field from another driven quantum system. *Phys. Rev. Lett.* **70**, 2269–2273 (1993).
56. C. Gardiner, P. Zoller, P. Zoller, *Quantum Noise: A Handbook of Markovian and Non-Markovian Quantum Stochastic Methods with Applications to Quantum Optics* (Springer Science & Business Media, 2004).

PNAS
www.pnas.org

Supplementary Information for

Induced transparency by interference or polarization

Changqing Wang, Xuefeng Jiang, William R. Sweeney, Chia Wei Hsu, Yiming Liu, Guangming Zhao, Bo Peng, Mengzhen Zhang, Liang Jiang, A. Douglas Stone and Lan Yang

Lan Yang.
E-mail: yang@seas.wustl.edu

This PDF file includes:

www.pnas.org/cgi/doi/10.1073/pnas.2012982118

Supporting Information Text

S1. Polarization effects on electromagnetically induced transparency (EIT) in directly coupled resonators

In a pair of directly coupled resonators (Fig. 1B in the main text), which lay the foundation of various studies on EIT (1–4) and non-Hermitian photonics (5–13), the polarization mismatch leads to a reduced coupling efficiency ($\kappa_{eff} = \kappa\cos(\Delta\phi)$) between the two resonator modes, which is derived as follow.

We assume the polarization states of the incoming light in the waveguide, WGM in μR_1 and WGM in μR_2 are P_0, P_1 and P_2, respectively. Each of them is represented by a 2-by-1 complex vector with unit length. Based on the temporal-coupled mode theory (TCMT) (14, 15), the rate equations of the filed amplitudes a_1 and a_2 of the two resonators are given by

$$\begin{aligned}\frac{d}{dt}a_1 =&(-i\omega_1 - \frac{\gamma_1+\gamma_{c1}}{2})a_1 - i\kappa a_2\,(P_1\cdot P_2)\\ &- \sqrt{\gamma_{c1}}a_{in}\,(P_0\cdot P_1)\,,\end{aligned} \quad [1]$$

$$\frac{d}{dt}a_2 =(-i\omega_2 - \frac{\gamma_2+\gamma_{c2}}{2})a_2 - i\kappa a_1\,(P_1\cdot P_2)\,. \quad [2]$$

This yields an effective non-Hermitian Hamiltonian

$$H = \begin{pmatrix}\omega_1 - i\frac{\gamma_1+\gamma_{c1}}{2} & \kappa_{eff}\\ \kappa_{eff} & \omega_2 - i\frac{\gamma_2+\gamma_{c2}}{2}\end{pmatrix}, \quad [3]$$

where the effective coupling strength is

$$\kappa_{eff} = \kappa\,(P_1\cdot P_2)\,. \quad [4]$$

For quasi-linear polarization states of WGMs, we assume the angle between P_1 and P_2 is $\Delta\phi$ which lies in the range $[0,\pi]$. Then we have

$$\kappa_{eff} = \kappa\cos(\Delta\phi)\,. \quad [5]$$

One can tell from the above analysis that the Hamiltonian of the directly coupled resonator system under polarization mismatch can be regarded as equivalent to those with matched polarization states, if we modify the coupling strength κ by $\cos(\Delta\phi)$. The cooperativity parameter (16) which describes the figure of merit of EIT becomes

$$\begin{aligned}C &= \frac{4\kappa_{eff}^2}{(\gamma_1+\gamma_{c1})(\gamma_2+\gamma_{c2})}\\ &= \frac{4\kappa^2\cos^2\Delta\phi}{(\gamma_1+\gamma_{c1})(\gamma_2+\gamma_{c2})},\end{aligned} \quad [6]$$

which decreases with larger polarization mismatch. Therefore the figure of merit of EIT is reduced by the polarization mismatch between the modes of the two resonators. On the other hand, the only component of the field in the waveguide that is involved in the EIT process is the component that is aligned with the polarization of the mode in μR_2. Assuming $P_0\cdot P_1 = \cos(\phi_1)\exp(i\theta)$, where $\theta = 0$ if both P_0 and P_1 are quasi-linear polarization states. Therefore, the other non-interacting component with amplitude $a_{in}\sin(\phi_1)$ will add a baseline onto the EIT lineshape in the transmission spectrum.

S2. General formalism describing scattering properties of indirectly coupled resonator systems

Here we treat the scattering of light through two taper-coupled resonators in series with mismatched resonant polarization states (see Fig. 1D in main text). The backscattering between clockwise (CW) and counterclockwise (CCW) modes leads to reflection and coupling between the two resonators (10, 17–19). This formalism will lay the foundation for all the scattering behavior we discuss in this study, including the polarization induced transparency, and the treatment of the system in the chiral case.

With a coordinate of polarization set up, there are four incident amplitudes, one for each polarization and side, which form a vector

$$\alpha = \begin{pmatrix}\lambda_1\\ \lambda_2\\ \rho_1\\ \rho_2\end{pmatrix}, \quad [7]$$

with $\lambda_{1(2)}$ being the left-incident amplitude with polarization 1 (2), and similarly with the ρ's being the right-incident amplitudes. These inputs are power-normalized, so that, e.g., $|\lambda_1|^2$ is the input power from the left in polarization 1.

The outgoing amplitudes are given by

$$\beta = \begin{pmatrix}\lambda_1'\\ \lambda_2'\\ \rho_1'\\ \rho_2'\end{pmatrix}, \quad [8]$$

and are related to the input by the scattering matrix

$$S = \begin{pmatrix} r_L & t_L \\ t_R & r_R \end{pmatrix}, \tag{9}$$

where r_L, r_R, t_L, t_R are all 2 by 2 matrices representing the reflection or transmission coefficients. Now we consider the scheme that two polarization controllers (PC1 and PC2) with unitary rotation matrices U_1 and U_2 are inserted between the input and μR$_1$, and between μR$_1$ and μR$_2$, respectively (Fig. S1). Each unitary matrix describing polarization mixing can be give as

$$U = \begin{pmatrix} e^{i\psi_1}\cos\Phi & -e^{i\psi_2}\sin\Phi \\ e^{-i\psi_2}\sin\Phi & e^{-i\psi_1}\cos\Phi \end{pmatrix}, \tag{10}$$

where $\psi_{1,2}$ are phases encoded in the rotation and Φ is the rotation angle. Consider the forward transmission, the matrix t_1 (t_2) is the transmission matrix of the taper-coupled resonator μR$_1$ (μR$_2$). r_{1L}/r_{1R} (r_{2L}/r_{2R}) represent the left/right reflection matrices of μR$_1$ (μR$_2$). Based on reciprocity, we can deduce that the backward transmission matrices for the two resonators are t_1^T and t_2^T, respectively. The scattering processes in the whole system can be described by the sets of equations as follow

$$\begin{pmatrix} \lambda' \\ a' \end{pmatrix} = \begin{pmatrix} 0 & U_1^T \\ U_1 & 0 \end{pmatrix} \begin{pmatrix} \lambda \\ a \end{pmatrix}, \tag{11}$$

$$\begin{pmatrix} a \\ b \end{pmatrix} = \begin{pmatrix} r_{1L} & t_1^T \\ t_1 & r_{1R} \end{pmatrix} \begin{pmatrix} a' \\ b' \end{pmatrix}, \tag{12}$$

$$\begin{pmatrix} b' \\ c' \end{pmatrix} = \begin{pmatrix} 0 & U_2^T \\ U_2 & 0 \end{pmatrix} \begin{pmatrix} b \\ c \end{pmatrix}, \tag{13}$$

$$\begin{pmatrix} c \\ \rho' \end{pmatrix} = \begin{pmatrix} r_{2L} & t_2^T \\ t_2 & r_{2R} \end{pmatrix} \begin{pmatrix} c' \\ \rho \end{pmatrix}, \tag{14}$$

where a, a', b, b', c and c' are defined as shown in Fig. S1. The reciprocity associated with each scattering process requires a symmetric scattering matrix, yielding $r_{iL} = r_{iL}^T$ and $r_{iR} = r_{iR}^T$ $(i = 1, 2)$. From Eqs. (11) and (12), we have

$$b = t_1 U_1 \lambda + r_{1R} U_2^T c. \tag{15}$$

From Eqs. (13) and (14), we get another relation

$$c = r_{2L} U_2 b + t_2^T \rho. \tag{16}$$

It follows that

$$c = \left(1 - r_{2L} U_2 r_{1R} U_2^T\right)^{-1} \left(r_{2L} U_2 t_1 U_1 \lambda + t_2^T \rho\right). \tag{17}$$

Plugging Eq. (17) back into Eqs. (11)-(14), we write every vector, including λ' and ρ', in terms of λ and ρ, so that we obtain the elements of the S matrix

$$\begin{aligned} r_L =& U_1^T t_1^T U_2^T \left(1 - r_{2L} U_2 r_{1R} U_2^T\right)^{-1} r_{2L} U_2 t_1 U_1 \\ &+ U_1^T r_{1L} U_1, \end{aligned} \tag{18}$$

$$r_R = t_2 U_2 r_{1R} U_2^T \left(1 - r_{2L} U_2 r_{1R} U_2^T\right)^{-1} t_2^T + r_{2R}, \tag{19}$$

$$t_L = U_1^T t_1^T U_2^T \left(1 - r_{2L} U_2 r_{1R} U_2^T\right)^{-1} t_2^T, \tag{20}$$

$$\begin{aligned} t_R =& t_2 U_2 r_{1R} U_2^T \left(1 - r_{2L} U_2 r_{1R} U_2^T\right)^{-1} r_{2L} U_2 t_1 U_1 \\ &+ t_2 U_2 t_1 U_1 \\ =& t_2 \left(1 - U_2 r_{1R} U_2^T r_{2L}\right)^{-1} U_2 t_1 U_1. \end{aligned} \tag{21}$$

We can see that

$$t_R^T = t_L, \tag{22}$$

which ensures a symmetric S matrix and the reciprocity of the polarization rotation processes.

S3. Derivation of polarization induced transparency (PIT)

We now come to a simple case that the resonators have no direct coupling; the taper and a polarization controller are the sole mediators between the two resonators. We also neglect any intracavity scattering between the CW and CCW modes within each resonator.

The serial nature of the system, together with the absence of back-scattering, implies that the scattering matrix has the representation

$$S = \begin{pmatrix} 0 & (t_2 U_2 t_1 U_1)^T \\ t_2 U_2 t_1 U_1 & 0 \end{pmatrix}. \quad [23]$$

The outgoing amplitudes are given by $\beta = S\alpha$, and therefore the total output power, $\beta^\dagger \beta$, is

$$I_{\text{out}} = \alpha^\dagger S^\dagger S \alpha. \quad [24]$$

From Eq. (23):

$$S^\dagger S = \begin{pmatrix} T^L & 0 \\ 0 & T^R \end{pmatrix}, \quad [25]$$

where $T^L \equiv t^\dagger t$, $T^R \equiv (tt^\dagger)^*$, and $t = t_2 U_2 t_1 U_1$. For example, T^L_{ii} is the total output when illuminating from the left with pure polarization i.

We assume that near the incident frequency ω, each resonator has a single resonance $\omega_{1,2} - i\gamma_{1,2}/2$ with a definite polarization which is different from either of the polarization states of the waveguide. For each resonator, there exists *some* polarization basis in which its coupling matrix is $\propto (1, 0)$ (we neglect the coupling to the backward-propagating channels). The basis in which this holds is connected to the waveguide polarization basis by a unitary transformation $V_{1,2}$. From the fundamental relation $S = I - 2iW^\dagger(\omega - H_{\text{eff}})^{-1}W$, where

$$H_{\text{eff}\,1,2} = \omega_{1,2} - i\gamma_{1,2}/2 - iW_{1,2}W^\dagger_{1,2}, \quad [26]$$

we see that if the polarization controllers are set to satisfy $U_1 = U_2^\dagger$, then their combined effect is to perform a unitary transformation on $W_1 \to W_1' = W_1 U_2^\dagger = (1, 0)V_1'$, where $V_1' = V_1 U_2^\dagger$ is also unitary. We assume from now on that the polarization controllers are so set, and include them in effective unitaries V_1', V_2, which are parameterized by angles $\phi_{1,2}$ and phases $\delta_{1,2}$, $\chi_{1,2}$. The effective coupling matrices (one for each resonator) in the waveguide polarization basis (choosing the polarization of the input light as the x direction) are:

$$W'_{1,2} = \sqrt{\frac{\gamma_{c1,2}}{2}}(e^{i\delta_{1,2}} \cos\phi_{1,2},\ e^{i\chi_{1,2}} \sin\phi_{1,2}), \quad [27]$$

where $W_2' = W_2$. Since we assume that the free propagation in the fiber is polarization-independent, we are free to choose the first polarization state to be parallel to the resonant polarization of the second cavity, i.e., $\phi_2 = 0$. Henceforth we write $\Delta\phi$ for ϕ_1.

The elements of the left-incident transmission matrix are

$$\begin{aligned} T^L_{11} =& \left(\frac{\Delta_1^2 + (\gamma_1 - \gamma_{c1})^2}{\Delta_1^2 + (\gamma_1 + \gamma_{c1})^2}\right)\left(\frac{\Delta_2^2 + (\gamma_2 - \gamma_{c2})^2}{\Delta_2^2 + (\gamma_2 + \gamma_{c2})^2}\right) \\ &+ \left\{\frac{4\gamma_2\gamma_{c1}\gamma_{c2}\cos^2\Delta\phi + \gamma_1[\Delta_2^2 + (\gamma_2 - \gamma_{c2})^2]}{[\Delta_1^2 + (\gamma_1 + \gamma_{c1})^2][\Delta_2^2 + (\gamma_2 + \gamma_{c2})^2]}\right\} \\ &\times 4\gamma_{c1}\sin^2\Delta\phi, \\ T^L_{22} =& 1 - \frac{4\gamma_1\gamma_{c1}\sin^2\Delta\phi}{\Delta_1^2 + (\gamma_1 + \gamma_{c1})^2} \\ &- \left(\frac{4\gamma_{c1}^2\sin^2\Delta\phi}{\Delta_1^2 + (\gamma_1 + \gamma_{c1})^2}\right)\left(\frac{4\gamma_2\gamma_{c2}\sin^2\Delta\phi}{\Delta_2^2 + (\gamma_2 + \gamma_{c2})^2}\right), \\ T^L_{12} =& -\frac{2e^{i(\delta_1 - \chi_1)}\sin(2\Delta\phi)}{[\Delta_1^2 + (\gamma_1 + \gamma_{c1})^2][\Delta_2^2 + (\gamma_2 + \gamma_{c2})^2]} \\ &\times \{2\gamma_2\gamma_{c2}[\gamma_{c1}\cos(2\Delta\phi) - i(\Delta_1 + i\gamma_1)] \\ &+ \gamma_1[\Delta_2^2 + (\gamma_2 - \gamma_{c2})^2]\}, \end{aligned} \quad [28]$$

where $\Delta_{1,2} \equiv \omega - \omega_{1,2}$. Note that $T^{L,R}_{12} = (T^{L,R}_{21})^*$.

The right-to-left transmission matrix T^R has elements

$$\begin{aligned} T_{11}^R =& \left(\frac{\Delta_1^2+(\gamma_1-\gamma_{c1})^2+4\gamma_1\gamma_{c1}\sin^2\Delta\phi}{\Delta_1^2+(\gamma_1+\gamma_{c1})^2}\right) \\ &\times\left(\frac{\Delta_2^2+(\gamma_2-\gamma_{c2})^2}{\Delta_2^2+(\gamma_2+\gamma_{c2})^2}\right), \\ T_{22}^R =& 1-\frac{4\gamma_1\gamma_{c1}\sin^2\Delta\phi}{\Delta_1^2+(\gamma_1+\gamma_{c1})^2}, \\ T_{12}^R =& 2e^{i(\delta_1-\chi_1)}\sin(2\Delta\phi)\left(\frac{\gamma_1\gamma_{c1}}{\Delta_1^2+(\gamma_1+\gamma_{c1})^2}\right) \\ &\times\left(\frac{\Delta_2-i(\gamma_2-\gamma_{c2})}{\Delta_2-i(\gamma_2+\gamma_{c2})}\right). \end{aligned} \quad [29]$$

Note that $T_{ij}^L \neq T_{ij}^R$. In particular, the difference between the outputs when illuminating from the left with polarization 1 and from the right with the same polarization 1 is

$$T_{11}^L - T_{11}^R = \frac{\gamma_{c1}^2\sin^2(2\Delta\phi)}{\Delta_1^2+(\gamma_1+\gamma_{c1})^2}\frac{4\gamma_2\gamma_{c2}}{\Delta_2^2+(\gamma_2+\gamma_{c2})^2}. \quad [30]$$

For the experiment described in the main text, in which $\gamma_1 \ll \gamma_2$ and the critical coupling condition is satisfied for the second resonator ($\gamma_2 = \gamma_{c2}$), we can then approximate the second factor to be unity in the frequency range $|\Delta_1| \ll \gamma_2$, and

$$T_{11}^L - T_{11}^R \approx \frac{\gamma_{c1}^2\sin^2(2\Delta\phi)}{\Delta_1^2+(\gamma_1+\gamma_{c1})^2}. \quad [31]$$

Therefore we expect a Lorentzian peak in the difference between the two, which will be modulated by $\sin^2(2\Delta\phi)$, which is the signature of PIT. Assuming ideal tuning (i.e., $\Delta\phi = \pi/4$), the peak output of the PIT will be $1/(1+\gamma_1/\gamma_{c1})^2$, so that stronger coupling of $\mu\mathrm{R}_1$ is preferred.

The asymmetry in the left and right transmission explains the unidirectional feature of PIT. It is noted that the reciprocity is still obeyed, which could be otherwise broken in the presence of thermally/mechanically/electrically-induced optical nonlinear effects (20–27). The narrow transparency window in Fig. 2D in the main text is due to the transmitted light with polarization perpendicular to P_0. The transmitted component in P_0 polarization is the same from both sides, following reciprocity. This is distinct from the Faraday effect (28) which leads to nonreciprocal light propagation based on the fact that the rotation of polarization of light is dependent on the magnetic field component in the direction of light propagation.

S4. Model of the indirectly coupled resonators with backscattering and polarization mismatch

We now discuss the indirectly coupled resonators with backscattering and polarization mismatch. Suppose that the CW and CCW modes in the resonator $\mu\mathrm{R}_1$ ($\mu\mathrm{R}_2$) are coupled by scatterers with coupling strengths κ_{a21} and κ_{a12} (κ_{b21} and κ_{b12}) (10, 18, 19). The modes in $\mu\mathrm{R}_1$ ($\mu\mathrm{R}_2$) are associated with a quasi-linear polarization states represented by P_1 (P_2), whose direction has an angle of ϕ_1 (ϕ_2) relative to the direction of P_0, which denotes the linear polarization of the input light also defined as the x direction. The scattering behavior of the system can be derived from the general form of the S matrix in Eq. (9), or can be directly described by the coupled mode equations involving polarization decomposition:

$$\begin{aligned} \frac{d}{dt}\begin{pmatrix}a_1\\a_2\end{pmatrix} =& \begin{pmatrix}-i\omega_1-\frac{\gamma_1+\gamma_{c1}}{2} & -i\kappa_{a21}\\ -i\kappa_{a12} & -i\omega_1-\frac{\gamma_1+\gamma_{c1}}{2}\end{pmatrix}\begin{pmatrix}a_1\\a_2\end{pmatrix} \\ &-\sqrt{\gamma_{c1}}\cos(\phi_1)\begin{pmatrix}a_{in}\\ e^{i\theta}b'_{outx}\end{pmatrix} \\ &-\sqrt{\gamma_{c1}}\sin(\phi_1)\begin{pmatrix}0\\ e^{i\Delta\phi}b'_{outy}\end{pmatrix}, \end{aligned} \quad [32]$$

$$\begin{pmatrix}a'_{outx}\\ b_{outx}\end{pmatrix} - \begin{pmatrix}a_{in}\\ e^{i\theta}b'_{outx}\end{pmatrix} = \sqrt{\gamma_{c1}}\cos(\phi_1)\begin{pmatrix}a_1\\a_2\end{pmatrix}, \quad [33]$$

$$\begin{pmatrix}a'_{outy}\\ b_{outy}\end{pmatrix} - \begin{pmatrix}0\\ e^{i\theta}b'_{outy}\end{pmatrix} = \sqrt{\gamma_{c1}}\sin(\phi_1)\begin{pmatrix}a_1\\a_2\end{pmatrix}, \quad [34]$$

$$\begin{aligned} \frac{d}{dt}\begin{pmatrix}b_1\\b_2\end{pmatrix} =& \begin{pmatrix}-i\omega_2-\frac{\gamma_2+\gamma_{c2}}{2} & -i\kappa_{b21}\\ -i\kappa_{b12} & -i\omega_2-\frac{\gamma_2+\gamma_{c2}}{2}\end{pmatrix}\begin{pmatrix}b_1\\b_2\end{pmatrix} \\ &-\sqrt{\gamma_{c2}}\cos(\phi_2)\begin{pmatrix}e^{i\theta}a'_{outx}\\ 0\end{pmatrix} \\ &-\sqrt{\gamma_{c2}}\sin(\phi_2)\begin{pmatrix}e^{i\theta}a'_{outy}\\ 0\end{pmatrix}, \end{aligned} \quad [35]$$

$$\begin{pmatrix} a_{outx} \\ b'_{outx} \end{pmatrix} - \begin{pmatrix} e^{i\theta} a'_{outx} \\ 0 \end{pmatrix} = \sqrt{\gamma_{c2}} \cos(\phi_2) \begin{pmatrix} b_1 \\ b_2 \end{pmatrix}, \quad [36]$$

$$\begin{pmatrix} a_{outy} \\ b'_{outy} \end{pmatrix} - \begin{pmatrix} e^{i\theta} a'_{outy} \\ 0 \end{pmatrix} = \sqrt{\gamma_{c2}} \sin(\phi_2) \begin{pmatrix} b_1 \\ b_2 \end{pmatrix}. \quad [37]$$

One can solve Eqs. (32)-(37) numerically in the frequency domain and steady states to obtain the transmission spectrum. In particular, in the case that $\omega_1 = \omega_2$ ($\Delta_1 = \Delta_2 = \Delta$) and P_2 aligns with P_0 ($\phi_2 = 0$, $\Delta\phi = \phi_1$) as shown in Fig. 4 of the main text, one can solve analytically that the transmission of the x component becomes

$$\begin{aligned} T_x &= |t_x|^2 = |a_{outx}/a_{in}|^2 \\ &= \left| \frac{(\Gamma_{1+}\Gamma_{1-} + \kappa_{a21}\kappa_{a12})(\Gamma_{2+}\Gamma_{2-} + \kappa_{b21}\kappa_{b12})}{Q + (\Gamma_{1+}^2 + \kappa_{a21}\kappa_{a12})(\Gamma_{2+}^2 + \kappa_{b21}\kappa_{b12})} \right|^2, \end{aligned} \quad [38]$$

where

$$\Gamma_{1\pm} = -i\Delta + \frac{\gamma_1 + \gamma_{c1}\sin^2(\Delta\phi)}{2} \pm \frac{\gamma_{c1}\cos^2(\Delta\phi)}{2}, \quad [39]$$

$$\Gamma_{2\pm} = -i\Delta + \frac{\gamma_2}{2} \pm \frac{\gamma_{c2}}{2}, \quad [40]$$

and

$$Q = \gamma_{c1}\cos^2(\Delta\phi)\gamma_{c2}\kappa_{a21}\kappa_{b12}e^{i\theta}. \quad [41]$$

The transmission of the y component is calculated as

$$\begin{aligned} T_y &= |t_y|^2 = |a_{outy}/a_{in}|^2 \\ &= \left| e^{i\theta}\sqrt{\gamma_{c1}}\sin(\Delta\phi)\, a_1/a_{in} \right|^2. \end{aligned} \quad [42]$$

We can calculate a_1 in the frequency domain by

$$\begin{pmatrix} a_1[\omega] \\ a_2[\omega] \end{pmatrix} = \sqrt{\gamma_{c1}}\cos(\Delta\phi)\, M^{-1} \begin{pmatrix} a_{in}[\omega] \\ e^{i\theta} b'_{outx}[\omega] \end{pmatrix}, \quad [43]$$

where

$$M = \begin{pmatrix} -\Gamma_1 & -i\kappa_{a21} \\ -i\kappa_{a21} & -\Gamma_1 \end{pmatrix}. \quad [44]$$

To evaluate Eq. (43), we note that

$$B_{outx}[\omega] = [1 - (M_2)_{2,1}(M_1)_{1,2}]^{-1} (M_2)_{2,1}(M_1)_{1,1} a_{in}[\omega], \quad [45]$$

where

$$M_1 = \begin{pmatrix} 1 - \frac{\gamma_{c1}\cos^2(\Delta\phi)\Gamma_1}{\Gamma_1^2 + \kappa_{a21}\kappa_{a12}} & -\frac{i\gamma_{c1}\cos^2(\Delta\phi)\kappa_{a21}e^{i\theta}}{\Gamma_1^2 + \kappa_{a21}\kappa_{a12}} \\ -\frac{i\gamma_{c1}\cos^2(\Delta\phi)\kappa_{a12}}{\Gamma_1^2 + \kappa_{a21}\kappa_{a12}} & e^{i\theta} - \frac{\gamma_{c1}\cos^2(\Delta\phi)\Gamma_1 e^{i\theta}}{\Gamma_1^2 + \kappa_{a21}\kappa_{a12}} \end{pmatrix}, \quad [46]$$

and

$$M_2 = \begin{pmatrix} e^{i\theta} - \frac{\gamma_{c2}\Gamma_2 e^{i\theta}}{\Gamma_2^2 + \kappa_{b21}\kappa_{b12}} & -\frac{i\gamma_{c2}\kappa_{b21}}{\Gamma_2^2 + \kappa_{b21}\kappa_{b12}} \\ -\frac{i\gamma_{c2}\kappa_{b12}e^{i\theta}}{\Gamma_2^2 + \kappa_{b21}\kappa_{b12}} & 1 - \frac{\gamma_{c2}\Gamma_2}{\Gamma_2^2 + \kappa_{b21}\kappa_{b12}} \end{pmatrix}. \quad [47]$$

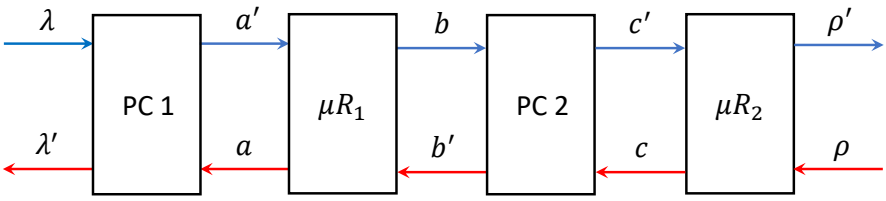

Fig. S1. Schematic diagram for deriving the general S matrix for the indirectly coupled resonator system.

References

1. DD Smith, H Chang, KA Fuller, A Rosenberger, RW Boyd, Coupled-resonator-induced transparency. *Phys. Rev. A* **69**, 063804 (2004).
2. K Totsuka, N Kobayashi, M Tomita, Slow light in coupled-resonator-induced transparency. *Phys. review letters* **98**, 213904 (2007).
3. H Jing, et al., Optomechanically-induced transparency in parity-time-symmetric microresonators. *Sci. reports* **5**, 9663 (2015).
4. W Li, Y Jiang, C Li, H Song, Parity-time-symmetry enhanced optomechanically-induced-transparency. *Sci. Reports* **6**, 31095 (2016).
5. B Peng, et al., Parity–time-symmetric whispering-gallery microcavities. *Nat. Phys.* **10**, 394–398 (2014).
6. B Peng, et al., Loss-induced suppression and revival of lasing. *Science* **346**, 328–332 (2014).
7. J Zhang, et al., A phonon laser operating at an exceptional point. *Nat. Photonics* **12**, 479–484 (2018).
8. R El-Ganainy, et al., Non-hermitian physics and pt symmetry. *Nat. Phys.* **14**, 11–19 (2018).
9. L Feng, R El-Ganainy, L Ge, Non-hermitian photonics based on parity–time symmetry. *Nat. Photonics* **11**, 752–762 (2017).
10. W Chen, C Wang, B Peng, L Yang, Non-hermitian physics and exceptional points in high-quality optical microresonators. *Ultra-high-q Opt. Microcavities*, 269–313 (2020).
11. H Hodaei, et al., Enhanced sensitivity at higher-order exceptional points. *Nature* **548**, 187–191 (2017).
12. WR Sweeney, CW Hsu, S Rotter, AD Stone, Perfectly absorbing exceptional points and chiral absorbers. *Phys. review letters* **122**, 093901 (2019).
13. S Assawaworrarit, X Yu, S Fan, Robust wireless power transfer using a nonlinear parity–time-symmetric circuit. *Nature* **546**, 387–390 (2017).
14. HA Haus, *Waves and fields in optoelectronics*. (Prentice-Hall, Englewood Cliffs, NJ), pp. 211–216 (1984).
15. HA Haus, W Huang, Coupled-mode theory. *Proc. IEEE* **79**, 1505–1518 (1991).
16. YC Liu, BB Li, YF Xiao, Electromagnetically induced transparency in optical microcavities. *Nanophotonics* **6**, 789–811 (2017).
17. J Zhu, et al., On-chip single nanoparticle detection and sizing by mode splitting in an ultrahigh-q microresonator. *Nat. photonics* **4**, 46 (2010).
18. B Peng, et al., Chiral modes and directional lasing at exceptional points. *Proc. Natl. Acad. Sci.* **113**, 6845–6850 (2016).
19. C Wang, et al., Electromagnetically induced transparency at a chiral exceptional point. *Nat. Phys.* **16**, 334–340 (2020).
20. D Jalas, et al., What is—and what is not—an optical isolator. *Nat. Photonics* **7**, 579–582 (2013).
21. T Carmon, L Yang, KJ Vahala, Dynamical thermal behavior and thermal self-stability of microcavities. *Opt. express* **12**, 4742–4750 (2004).
22. Y Li, X Jiang, G Zhao, L Yang, Whispering gallery mode microresonator for nonlinear optics. *arXiv preprint arXiv:1809.04878* (2018).
23. X Jiang, L Yang, Optothermal dynamics in whispering-gallery microresonators. *Light. Sci. & Appl.* **9**, 1–15 (2020).
24. Y Liu, X Jiang, C Wang, L Yang, Optothermally induced mechanical oscillation in a silk fibroin coated high-q microsphere. *Appl. Phys. Lett.* **116**, 201104 (2020).
25. YL Liu, et al., Controllable optical response by modifying the gain and loss of a mechanical resonator and cavity mode in an optomechanical system. *Phys. Rev. A* **95**, 013843 (2017).
26. L Shao, et al., Non-reciprocal transmission of microwave acoustic waves in nonlinear parity–time symmetric resonators. *Nat. Electron.*, 1–6 (2020).
27. W Chen, D Leykam, YD Chong, L Yang, Nonreciprocity in synthetic photonic materials with nonlinearity. *MRS Bull.* **43**, 443–451 (2018).
28. L Aplet, J Carson, A faraday effect optical isolator. *Appl. Opt.* **3**, 544–545 (1964).